Section A-Research paper

ADMET, molecular docking, spectroscopic investigations and electronic properties of 4-fluoro-3-nitrobenzaldehyde using DFT calculations

S. Jeyavijayan[1,*], A. Shiney[2], M. Ramuthai[3], K.Vinoth[4], S. Prabhakaran[5]

[1]Department of Physics, Kalasalingam Academy of Research and Education, Krishnankoil- 626 126, Tamil Nadu, India

[2]Department of Physics, Pocker Sahib Memorial Orphanage College, Tirurangadi, Malappuram, Kerala-676306, India

[3]Department of Physics, Arumugham Palaniguru Arts & Science College, Chatrapatti-626 102, Tamil Nadu, India

[4]Department of Physics, J.J. College of Engineering and Technology, Tiruchirappalli-620 009, India

[5]Department of Physics, Jamal Mohamed College, Tiruchirappalli-620 020, India

*E-mail: sjeyavijayan@gmail.com

Abstract

The experimental and theoretical FTIR, FT-Raman spectra of 4-fluoro-3-nitrobenzaldehyde (FNB) were investigated extensively using density functional theory (DFT) technique. The total energy distribution (TED) confirms the contributions of various modes. The geometric and thermodynamic parameters of FNB have been computed. The small HOMO-LUMO energy gap explains the interaction of charge transfer of FNB. Natural bond orbital (NBO) study elucidates the charge delocalization of the molecule. The Mulliken's plot and mapped molecular electrostatic potential (MEP) have also been reported. The results of docking showed that the FNB molecule has the maximum binding energy (-6.0 kcal/mol) with the aldehyde dehydrogenases (ALDHs). To recognize the molecule's drug image, ADMET (Absorption, Distribution, Metabolism, Excretion, Toxicity) studies have also been considered.

Keywords: FTIR; FT-Raman; DFT calculations; 4-fluoro-3-nitrobenzaldehyde; ADMET

1. Introduction

The derivatives of benzaldehyde such as anisaldehyde, vanillin and hydroxybenzaldehyde are active in the production of bioactive agents which have extensive usage in pharmaceuticals cosmetics and textiles [1-3]. They are also useful as a main originator to many numbers of pharmaceutical compounds. In current years, several theoretical and experimental works have been done on the vibrational properties of benzaldehyde derivatives [4-9]. Recently, the spectral studies of derivatives of benzaldehyde thiosemicarbazone as corrosion inhibitors have been investigated by Zhang et al. [10]. Also, the vibrational investigations of benzaldehyde derivatives are very important for the understanding of exact biological process and in the investigation of complex molecular systems. Further, in the DFT methods, Becke's 3 parameter hybrids functional joint with the correlation functional of Lee-Yang-Parr (B3LYP) includes numerous exchange and correlation functionals, thus provides best outcomes for molecular geometry and wave numbers even for huge molecular structures [11]. In the study, the vibrational spectra are compared with the B3LYP results for 4-fluoro-3-nitrobenzaldehyde (FNB) to get details about its intramolecular charge transfer, electronic properties and biological applications.

2. Experimental details

The infrared spectrum of FNB at room temperature was observed in the wavenumber between 4000-400 cm^{-1} and FT-Raman was noted in the wavenumber 3500–50 cm^{-1}. For the FTIR spectrum, the Perkin Elmer spectrometer armed with an MCT detector, globar source and KBr beam splitter have been used. Similarly, the BRUKER RFS-66V model interferometer and the source of Nd:YAG laser of wavelength 1064 nm with 200 mW power was used for excitation.

3. Computational details

Quantum chemical density functional theory calculations were carried out for FNB with the 2009 Window type of the GAUSSIAN suite program [12] using Becke-3-Lee-Yang-Parr functional (B3LYP) [13,14] accompanied with the basis sets B3LYP/6-31+G(d,p) and B3LYP/6-311++G(d,p). All the factors involved in the calculations were permitted to converge for an optimized geometry which matches to energy minimum. Scaled quantum mechanical (SQM) procedure [15] has been followed for good agreement between the experimental data and computational results. The vibrational frequencies and electronic parameters of FNB are calculated and the performance of the B3LYP computational method is carried out based on SQM approach. The Version V7.0-G77 of MOLVIB Program by Tom Sundius [16] has been utilized in the Total energy distribution (TED) calculation.

3.1 Molecular docking and ADMET prediction

Protein structures (PDB ID: 5FHZ, 4H80) are obtained by the protein bank (http://www.pdb.org) [17]. The selected FNB ligand molecule was found from PubChem datafiles: (http://pubchem.ncbi.nlm.nih.gov/). Then, the protein structure and amino acid interaction have been visualized by Discovery Studios (Adaptation: 2017 R2 client) [18] and Auto Dock Vina tool (Adaptation: 4.2.1) [19].

ADMET drug-likeness of FNB has been predicted using computational techniques. The toxicity of FNB was estimated by means of the pkCSM-pharmacokinetics server (http://biosig.unimelb.edu.au/pkcsm/prediction) and the ADMET-SAR estimation tool (http://lmmd.ecust.edu.cn/admetsar2/) [20].

4. Results and Discussion

4.1 Geometry analysis and symmetry

The molecular structure of FNB fits to C_1 point group is exposed in Fig. 1. The geometrical parameters of FNB are revealed in Table 1 and they are the sources for computing other parameters. The minimum energy found by the optimization through the basis sets 6-31+G(d,p) and 6-311++G(d,p) are -649.48592104 and -649.48607104 Hartrees, respectively.

Because of substitutions of fluorine atom, NO_2 and -HC=O groups in FNB, the benzene ring seems disturbed slightly and angles are deviated from the regular hexagonal structure. From the experimental values [21-22], the order of six C–C bond lengths of the ring are as C2–C3 < C4–C5 < C3–C4 < C5–C6 < C6–C1 < C1–C2. However, according to the calculated values (B3LYP/6-311++G (d,p)), the bond lengths is somewhat differed as C5–C6 < C2–C3 < C1–C2 < C4–C5 < C3–C4 < C6–C1, due to different substitutions. The C-C bond of the benzene ring C1–C6, C3–C4 and C4–C5 at the substitution place are 1.403, 1.398 and 1.393 Å, respectively, and they are lengthier than remaining bonds in the ring. Similarly, the C1-C7, C–F and C-N bond lengths are obtained as 1.484, 1.332 and 1.475 Å by B3LYP/6-311++G (d,p), which are deviated from the experimental value (1.480, 1.362 and 1.471 Å), respectively. The variations in the geometrical parameters and regular hexagonal structure of the ring are ascribed to the fluctuations in charge distribution of the ring carbons due to fluorine and nitrogen atoms. From the DFT results, the angles C2–C1–C6, C2–C3–C4 and C3–C4–C5 are deviated by 0.73^0, 3.15^0 and 1.35^0 from 120^0, respectively, at the atoms C1, C3 and C4 which reveal the repulsion between -HC=O, nitro groups, fluorine atom and the benzene ring. The order of angles C4–C5–C6 < C6–C1–C2 < C2–C3–C4 < C1–C2–C3 < C5–C6–C1 < C3–C4–C5 also showed the irregularity of the benzene ring.

4.2 Vibrational spectral analysis

FNB consists of 16 atoms which results 42 modes of vibrations and the complete normal mode reports by TED for FNB are reported in Table 2. The observed and calculated vibrational spectra of FNB are shown in Figs. 2 and 3, respectively. In this study, DFT calculations were completed for a molecule in vacuum, however experiments were achieved for solid sample. This creates inconsistency between calculated and observed vibrational wave numbers. Therefore, the calculated results were scaled by 0.9613 (scaling factor) for B3LYP method [23]. The scaled vibrational frequencies are recorded in Table 2.

4.2.1 C-H vibrations

The typical region for the C-H stretching vibrations in aromatic hetero structure [24] appears in the region 3000–3100 cm^{-1}. Here, the bands are unaltered expressively by the environment of substituent. The C-H stretching modes typically occur with solid Raman intensity and are extremely well polarized. Due to this high polarization, Raman bands have not been detected in the observed spectra. The FTIR bands observed at 3094, 3085, 3072 cm^{-1} and FT-Raman counterpart at 3087 cm^{-1} are assigned to the C-H stretching vibrations of FNB. The resultant force constant contributes almost 100% to the energy distribution. The C-H in-plane vibrations generally occur in the range 1000-1300 cm^{-1} in the benzene's derivatives and the out-of-plane C-H bending vibrations appear in the 750-1000 cm^{-1} region [24]. Hence, in the present case, the C-H in-plane vibrations are attributed to 1135, 1078, 1009, 984 in IR and 1124, 1084, 1010 cm^{-1} in the Raman. The C-H out-of-plane bending frequencies are assigned at 927, 903, 812, 774 cm^{-1} in FTIR and 927, 898, 775 cm^{-1} in the FT-Raman.

4.2.2 C-C vibrations

The C-C stretching vibrations in the benzene ring systems typically fall in 1625–1400 cm^{-1} [25]. In this study, the C-C stretching vibrational wavenumbers are detected at 1614, 1422, 1305 cm^{-1} in FTIR and 1647, 1614, 1438, 1317, 1210 cm^{-1} in FT-Raman spectrum. The C-C bending vibrations are assigned which are in good agreement with the literature [25] and also established by their TED values. Further, the substitutions fluorine atom, NO_2 and -HC=O groups interrupt the ring vibrations.

4.2.3 C-F vibrations

The C-F vibrations are easily affected by neighboring atoms and therefore they [26] may be originated over a wide wavenumber range 1000-1360 cm^{-1}. In the FTIR spectrum, the band observed at 1203 cm^{-1} has been allocated to C-F stretching vibration for FNB, which further support the TED (72%). The C-F bending vibrations are also assigned and recorded in the Table 2.

4.2.4 Aldehyde group vibrations

Aldehydes contain the carbonyl group (C=O) and its functional group is -HC=O. In the C=O group, the carbon atom is in sp^2 hybridization and the *pi* bond of -C=O group is made by the overlap of carbon atoms and p orbitals of oxygen. This creates two sp^2 hybrid orbitals in carbon atoms for bond formation, and the s and p orbitals on oxygen comprising the two electron lone pairs. Generally, the aldehydes carbonyl (C=O) stretching arises in the region 1740-1720 cm^{-1}. The C-H stretching in aldehydes usually appears as weak doublet in the region 2795-2030 cm^{-1}. Accordingly, the carbonyl (C=O) stretching in aldehyde is observed at 1699 cm^{-1} in IR, 1701 cm^{-1} in Raman and the aldehyde C-H stretching vibration for FNB found at 2867 cm^{-1} in both IR and Raman spectra. All these vibrations of aldehyde group are found in good consistency with the literature [27].

4.2.5 C-N vibrations

The C-N vibrations are actually tough task because of mixing of many bands are possible [28] and the C-N stretching bands for aromatic compounds are assigned in the 1266-1382 cm^{-1} region. In FNB, the band detected at 1256 and 1259 cm^{-1} in the vibrational spectra, are allocated to C=N stretching and its force constant contribute 72% TED. In FNB, the bands found at 526 and 528 cm^{-1} are assigned to C-N in-plane vibrations of FNB. The out-of-plane C-N vibration has also been allotted and is recorded in Table 2.

4.2.6 Nitro group vibrations

The NO_2 group vibrations basically have 6 fundamentals namely, NO_2 asymmetric stretch; NO_2 symmetric stretch; NO_2 scissoring; NO_2 wagging; NO_2 rocking; and NO_2 twisting mode. The NO_2 asymmetric stretching is normally detected in the region 1510-1485cm^{-1}, whereas the symmetric stretch will seem between 1370 and 1320 cm^{-1}. In this study, the NO_2 asymmetric vibrations of FNB are observed at 1529 and 1531 cm^{-1}. The NO_2 symmetric stretching is also identified at 1355 and 1357 cm^{-1} in the experimental spectra for FNB. The other vibrations of NO_2 group are also found fit with the typical region [29] and are summarized in Table 2.

4.3 HOMO-LUMO band gap and electronic spectral analysis

The biochemical stability of the molecule can be understood by the highest occupied and lowest unoccupied molecular orbitals molecular orbital (HOMO-LUMO) [30]. The HOMO and LUMO signifies the capability to donate and accept an electron, respectively. The HOMO and LUMO plot for FNB are showed in Fig. 4. The energy gap for FNB is found to be 4.681 eV, which exposes the charge transfer interactions occur of FNB. The HOMO is sited over the -HC=O group, LUMO is located over the NO_2 group, fluorine atom. Therefore, the HOMO-

LUMO transition suggests an electron cloud transfer to the fluorine atom, ring, NO_2 group from -HC=O group.

The oscillation strength (f), electronic transitions and excitation energies (E) of FNB were calculated by TDDFT method [31]. The UV spectrum of FNB is represented in Fig. 5. A solid peak is calculated at 399.85 nm by energy E = 3.1008 eV and frequency of 0.0041 for FNB. This equivalent to the $\pi \rightarrow \pi^*$ major transition from HOMO-2 to LUMO (contribution of 92%) as listed in Table 3.

4.4 NBO analysis

NBO investigation describes the conjugative interaction between the filled and virtual orbitals which is useful to get information about the intra and inters molecular interactions [32]. Larger the stabilization E(2) energy value, more rigorous interaction take place between the electron acceptors and donors. NBO analysis of FNB has been performed at the DFT/B3LYP level in order to clarify charge transfers, delocalization and intra-molecule rehybridization. The 2^{nd} order perturbation NBO analyses for FNB are presented in the Table 4. The n-π conjugation among the oxygen, fluorine lone pair electrons and benzene ring (π system) is very strong in the ground state. The $n2(O_8) \rightarrow \sigma^*(C_7 - H_9)$, $n2(O_{12}) \rightarrow \sigma^*(C_3 - N_{11})$, $n2(O_{13}) \rightarrow \sigma^*(C_3 - N_{11})$, $n3(F_{14}) \rightarrow \pi^*(C_3 - C_4)$ stabilization energies are 11.44, 6.60, 6.72 and 11.41 kJ cal^{-1}, respectively, shows n-π, n-σ conjugation among oxygen, fluorine atom and benzene ring. The remarkable interactions in FNB are $\pi^*(C_3\text{-}C_4) \rightarrow \pi^*(C_1\text{–}C_2)$, $\pi^*(C_3\text{-}C_4) \rightarrow \pi^*(C_5\text{–}C_6)$ and $\pi^*(N_{11}\text{–}O_{12}) \rightarrow \pi^*(C_3\text{–}C_4)$, these stabilization interactions results enormous energy of 59.68, 52.04 and 8.39 kJ cal^{-1}, respectively. Therefore, the FNB molecule is stabilized by these molecular orbital interactions which induce its bioactivity.

4.5 Thermodynamic properties

The thermodynamic parameters like entropy, heat capacity, rotational constants and zero point vibrational energy (ZPVE) are measured and are listed in Table 5. The scale factor has been proposed [33] for an exact calculation in defining the ZPVE and entropy. All these thermodynamic parameters are very much useful for additional study of FNB. They can be used to determine other thermodynamic energies and to evaluate the direction of chemical reactions.

4.6 Mulliken's population and NMR analysis

The charge distribution of any molecule plays a vital effect in the vibrational spectra [34]. The Mulliken atomic charges of FNB are enumerated in Table 6 and the corresponding plot is shown in Fig. 6. The results indicate that the substitution of fluorine atom, NO_2 and -HC=O groups in the benzene ring leads to electron density redistribution. Comparison of the charges calculated at different basis sets exposes the overestimation of charges due to the negligence of anharmonicity. The C1 carbon bonded by the aldehyde group has the more positive charge (1.1489 by larger basis set) compare to other ring carbon atoms.

The ^{13}C and ^{1}H NMR spectra for FNB have been applied by the B3LYP/6-311++G (d,p) through GIAO method [35]. This is the active way to infer the assembly of vast biomolecules as a reference tetramethyl silane (TMS) and is shown in Table 7. The calculated chemical spectra have been exposed in Fig. 7. Here, the calculated ^{13}C NMR shifts are noted from 123.30 to 191.73 ppm. Hence, the maximum shift is found for C7 (191.73) due to the electronegative belongings of oxygen atom (O8). The computed chemical shifts for H9 attached straight to oxygen have the extreme value of 10.14 ppm.

4.7 Molecular electrostatic potential

The electro and nucleophilic attacks [36] for FNB can be obtained from B3LYP/6-311++G(d,p) and its picture is shown in Fig. 8. Here, the negative potential is dispersed over the

nitro group, oxygen atom of -HC=O group and is represented by means of a yellowish blob, the positive potential is spread over the remaining portion of FNB. Here, the potential energy rises from red < orange < yellow < green < blue. In FNB, the negative potentials are on oxygen (Red-strongest repulsion) atoms and the positive potentials are nearby the hydrogen (Blue-strongest attraction) atoms.

4.8 ADMET prediction

In FNB, the LD50 of 2.294 mol/kg has been proved. In this work, the human oral absorption of FNB is known as 94.423%. Furthermore, the accepted range for the blood brain barrier (BBB) [20] is -3.0 to 1.2; remarkably, the molecule FNB shows the BBB permeability of -0.236 and the results indicating that the title molecule has good drug-like properties. Numerous ADMET limitations have also been obtained for FNB and are exposed in Table 8.

4.9 Molecular docking (MD)

ALDHs have also been associated with cancer therapy. Because of their metabolic and detoxifying abilities an increased ALDH expression can have a chemoprotective impact on cells [37]. Docked into the two studied isoforms (ALDH1A3 and ALDH3A1), with all results illustrated in Figs. 9(a), 9(b) and binding sites, interaction residues are shown in Tables 9(a), 9(b). From the docking analysis of ALDH1A3 (Figs. 9a, 9b), the aldehyde oxygen of O8 was found to form an H-bond with ARG B:96, and the benzene ring recognized face-to-face π–π interaction with PRO C:157. One of the NO_2 substituted group chain well-known obtained to form an H-bond with THR C:155, GLY B:153, HIS B:168 and van der Waals associates with ARG B:167. The inhibition action of ALDH1A3 has the maximum binding with FNB and is noted as -6.0 kcal mol^{-1} is shown in (Tables 9a, 9b). Similar protein-ligand interactions of ALDH3A1, the presence of NO_2 and Aldehyde oxygen group in the place of a H-bond interaction with the HIS G:423, GLY C:405. The Benzene ring established π - Alkyl interactions

with LEU G:104, PRO G:205 to higher binding energy with the target 5.8 kcal/mol represented in Figs. 9a, 9b and Tables 9a, 9b.

5. Conclusions

The optimized parameters and vibrational bands of 4-fluoro-3-nitrobenzaldehyde have been examined by B3LYP/6-31+G(d,p) and B3LYP/6-311++G(d,p) calculations accompanied by the experimental spectra. The outcomes of DFT-B3LYP indicate good fitting with experimental values. The influence of nitro, aldehyde groups and fluorine in FNB are also discussed. The HOMO-LUMO gap and NBO analysis elucidates the intramolecular charge transfer which is responsible for biological action. The Mulliken charge analysis describes the reorganization of electron distribution of FNB and the MEP surface expects the relative sites for the nucleophilic (oxygens) and electrophilic (hydrogens) attacks. ALDHs inhibitory confirmed that the molecule FNB is a potential bioactive agent with ALDHs which results higher binding energy (-6.0 $kcalmol^{-1}$). Highest LD50 results propose that the molecule have minimum toxicity. Therefore, both experimental and calculated studies clearly reveal that the molecule FNB has strong inhibitory activity against ALDH protein. 4-fluoro-3-nitrobenzaldehyde is proven to be successful in the treatment of aggressive ALDH expressing.

References

[1] C. Echeverria, J.F. Santibañez, O. Donoso-Tauda, C.A. Escobar and R. Ramirez-Tagle, Int J Mol Sci 10 (2009) 221-231.

[2] S. Vogel, M. Barbic, G. Jürgenliemk and J. Heilmann, Eur J Med Chem 45 (2010) 2206-2213.

[3] C.S.C. Kumar, W.S. Loh, C.W. Ooi, C.K. Quah and H.K. Fun, Molecules 18 (2013) 12707-12724.

[4] S. Gunasekaran and S. Ponnusamy, Indian J Pure & App Physics 43, (2005) 838-843.

[5] B.S. Yadav, S.K. Tyagi and Seema, Indian J Pure & App Physics 44 (2006) 644-648.

[6] C.S. Hiremath and Tom Sundius, Spectrochim Acta 74A (2009) 1260-1267.

[7] V. Karunakaran & V. Balachandran, Spectrochim Acta, 98A (2012) 229-239.

[8] P. Vennila, M. Govindaraju, G. Venkatesh and C. Kamal, J Mol Struct 1111 (2016) 151-156.

[9] N. Jeeva Jasmine, C. Arunagiri, A. Subashini, N. Stanley and P. Thomas Muthiah, J Mol Struct 1130 (2017) 244-250.

[10] A.D. Becke and J. Chem, Phys., 98 (1993) 5648-5652.

[11] C. Lee, W. Yang and R.G. Parr, Phys. Rev., 37 (1988) 785-789.

[12] M.J. Frisch, G.W. Trucks, H.B. Schlegal, G.E. Scuseria, M.A. Robb, J.R. Cheesman, V.G. Zakrzewski, J.A. Montgomerg, Jr., R.E. Stratmann, J.C. Burant, S. Dapprich, J.M. Millam, A.D. Daniels, K.N. Kudin, M.C. Strain, O. Farkas, J. Tomasi, V. Barone, M. Cossi, R. Cammi, B. Mennucci, C. Pomelli, C. Adamo, S. Clifford, J. Ochterski, G.A. Petersson, P.Y. Ayala, Q. Cui, K. Morokuma, N. Rega, P. Salvador, J.J. Dannenberg, D.K. Malich, A.D. Rabuck, K. Raghavachari, J.B. Foresman, J. Cioslowski, J.V. Ortiz, A.G. Baboul, B.B. Stetanov, G. Liu, A. Liashenko, P. Piskorz, I. Komaromi, R. Gomperts, R.L. Martin, D.J. Fox, T. Keith, M.A. Al-Laham, C.Y. Peng, A. Nanayakkara, M. Challacombe, P.M.W. Gill, B. Johnson, W. Chen, M.W. Wong, J.L. Andres, C. Gonzalez, M. Head-Gordon, E.S. Replogle and J.A. Pople, GAUSSIAN 09, Revision A 11.4, Gaussian, Inc, Pittsburgh PA, (2009).

[13] A.P Wieczorkiewicz, H. Szatylowicz, and T.M. Krygowski, Struct. Chem., 32 (2021) 915-923.

[14] D.A. Kleinman, Phys Rev., 126 (1962) 1977-1979.

[15] M.C. Ventura, E. Kassab, G. Buntinx, and O. Poizat, Phys. Chem. Chem. Phys., 20 (2000) 4682-4689.

[16] MOLVIB (V.7.0), Calculation of Harmonic Force Fields and Vibrational Modes of Molecules QCPE Program No. 807, (2002).

[17] M. Uma Priya, S. Kunjiappan, P.B.T. Pichiah, and S. Arunachalam, 3 Biotech 11 (2021) 1-13.

[18] B.L. Narayana, D. Pran Kishore, C. Balakumar, K.V. Rao, R. Kaur, A.R. Rao, J.N. Murthy and M. Ravikumar, Chem. Biol. Drug Des., 79 (2012) 674-682.

[19] O. Trott and A.J. Olson, J. Comput. Chem 31 (2010) 455-461.

[20] W. Guerrab, M. Jemli, J. Akachar, G. Demirtaş, J. T. Mague, J. Taoufik, A. Ibrahimi, M. Ansar, K. Alaoui and Y. Ramli, J. Biomol. Struct. Dyn 40 (2022) 8765-8782.

[21] A.H.J. Engwerda, S.J.T. Brugman, P. Tinnemans and E. Vlieg, IUCr 75, 38-45 (2018).

[22] R.E. Tureski and J.M. Tanski, Acta Cryst, 69 (2013) 1246-1246.

[23] D.C. Young, Computional Chemistry: A Pratical Guide for Applying Techniques to Real-World Problems, John Wiley & Sons, Inc., New York, (2001).

[24] K. Gomathi, R. Rathikha, and P. Rajesh, Eur. Chem. Bull., 12(5) (2023) 3516-3539.

[25] V. Krishnakumar and N. Prabavathi. Spectrochim. Acta A Mol. Biomol. Spectrosc., 71 (2008) 449-457.

[26] P. Venkata Ramana Rao, K. Srishailam, L. Ravindranath, B. Venkatram Reddy and G. Ramana Rao, J Mol Struct 1180 (2019) 142-151.

[27] V. Krishnakumar and V. Balachandran, Spectrochim Acta 63A (2006) 918-925.

[28] M. Arivazhagan, S. Jeyavijayan and J. Geethapriya, Spectrochim Acta 104 (2013) 14-25.

[29] M. Arivazhagan and S. Jeyavijayan, Indian J Pure & App Physics 49 (2011) 516-522.

[30] S. Jeyavijayan, Spectrochim. Acta A Mol. Biomol. Spectrosc., 136 (2015) 553-566.

[31] Fouegue, A.D. Tamafo, J.H. Nono, N.K. Nkungli and J.N. Ghogomu, Struct. Chem., 32(1) (2021) 353-366.

[32] S. Jeyavijayan and Palani Murugam, Asian J. Chem., 33(1) (2021) 83-88.

[33] M. Alcolea Palafox, Int J Quant Chem 77 (2000) 661-684.

[34] S. Jeyavijayan, Palanimurugan, K. Viswanathan, V. Lavanya and K. Gurushankar, Rasayan J. Chem., 12(2) (2019) 921-938.

[35] Palanimurugan and S. Jeyavijayan, Rasayan J. Chem., 14(1), (2021) 389-396.

[36] S. Jeyavijayan, M. Ramuthai and Palani Murugam, Asian J. Chem., 33 (2021) 2313-2320.

[37] A.I. Ibrahim, E. Batlle, S. Sneha, R. Jiménez, R. Pequerul, X. Parés, T. Rüngeler, V. Jha, T. Tuccinardi, M. Sadiq and F. Frame, J. Med. Chem., 65 (2022) 3833-3848.

Table 1 Geometrical parameters of 4-fluoro-3-nitrobenzaldehyde

Parameters	Method/Basis set		Experimental[21,22]
	B3LYP/ 6-31+G(d,p)	B3LYP/ 6-311++G(d,p)	
Bond length (Å)			
C1-C2	1.392	1.392	1.399
C2-C3	1.391	1.391	1.384
C3-C4	1.398	1.398	1.393
C4-C5	1.393	1.393	1.391
C5-C6	1.385	1.385	1.394
C6-C1	1.403	1.403	1.397

C1-C7	1.484	1.484	1.480
C7-O8	1.209	1.209	1.215
C7-H9	1.109	1.109	0.950
C2-H10	1.084	1.084	0.950
C3-N11	1.475	1.475	1.471
N11-O12	1.225	1.225	1.226
N11-O13	1.220	1.220	1.227
C4-F14	1.332	1.332	1.362
C5-H15	1.083	1.083	0.950
C6-H16	1.084	1.084	0.950
Bond angle (^{0})			
C1-C2-C3	120.15	120.16	117.39
C2-C3-C4	119.68	119.68	123.15
C3-C4-C5	120.48	120.48	118.65
C4-C5-C6	119.61	119.61	119.72
C5-C6-C1	120.38	120.39	120.36
C6-C1-C2	119.67	119.67	120.73
C1-C7-H9	114.82	114.82	117.9
C1-C7-O8	124.14	124.14	124.13
H9-C7-O8	121.04	121.03	117.9
C2-C1-C7	119.66	119.66	120.56
C6-C1-C7	120.67	120.67	118.69
C1-C2-H10	121.30	121.30	121.3
C3-C2-H10	118.54	118.54	121.3
C2-C3-N11	118.29	118.28	118.48
C4-C3-N11	122.03	122.04	118.36
C3-N11-O12	116.68	116.68	117.92
C3-N11-O13	117.81	117.81	118.29
O12-N11-O13	125.50	125.50	123.79
C3-C4-F14	121.37	121.38	118.63
C5-C4-F14	118.12	118.11	117.97
C4-C5-H15	118.41	118.41	120.1
C6-C5-H15	121.98	121.98	120.1
C5-C6-H16	120.83	120.83	119.8
C1-C6-H16	118.78	118.78	119.8

Table 2 The vibrational frequencies (cm^{-1}), Raman Activity ($Å^4$ amu^{-1}), IR intensity (Km mol^{-1}) and possible assignments for 4-fluoro-3-nitrobenzaldehyde

S.No.	Observed wave number (cm^{-1})		Calculated frequencies (cm^{-1})								TED% among types of coordinates
			B3LYP/6-31+G(d,p)				B3LYP/6-311++G(d,p)				
	FTIR	FT Raman	Unscaled	Scaled	IR intensity	Raman active	Unscaled	Scaled	IR intensity	Raman active	
1	3094(w)	-	3208	3079	1.74	161.47	3207	3079	1.74	161.80	νCH(99)
2	3085(w)	3087(ms)	3198	3070	2.89	50.20	3198	3070	2.95	49.09	νCH(97)
3	3072(ms)	-	3195	3067	0.70	33.19	3195	3067	0.70	33.82	νCH(96)
4	2867(ms)	2867(w)	2911	2794	84.78	122.65	2910	2794	84.94	125.42	νCH(92)
5	1699(vs)	1701(s)	1777	1705	283.42	127.59	1776	1705	283.37	127.41	νCO(79), bCH(13)
6	-	1647(s)	1652	1585	267.36	56.60	1652	1585	267.23	56.65	νCC(78), bCN(18)
7	1614(s)	1614(ms)	1621	1557	73.82	30.76	1621	1557	73.81	30.78	νCC(77), bCH(14)
8	1529(vs)	1531(ms)	1594	1531	143.79	57.14	1594	1531	143.73	57.19	NO_2ass(85), bCC(14)
9	-	1438(vw)	1524	1463	18.29	2.94	1523	1463	18.25	2.94	νCC(80), bCH(17)
10	1422(ms)	-	1446	1388	5.38	2.07	1446	1388	5.37	2.03	νCC(76), Rtrigd(23)
11	1355(vs)	1357(vs)	1405	1348	8.26	3.87	1404	1348	8.39	3.94	NO_2ss(74),bCN(22)
12	-	1317(vw)	1374	1319	295.51	96.77	1374	1319	295.83	96.72	νCC(80), bCC(13)
13	1305(vw)	-	1348	1294	7.70	2.12	1348	1294	7.76	2.11	νCC(78), bCH(22)
14	1256(vs)	1259(ms)	1285	1233	4.02	1.37	1285	1233	3.99	1.39	νCN(72), bCC(12)
15	-	1210(ms)	1273	1222	139.44	57.25	1273	1222	139.53	57.43	νCC(74), NO_2ss(15)
16	1203(s)	-	1217	1168	55.27	32.29	1217	1168	55.08	32.25	νCF(72), bCC(20)
17	1135(ms)	1124(w)	1153	1107	12.70	7.22	1153	1107	12.82	7.24	bCH(74),bCC(19)
18	1078(s)	1082(vw)	1095	1051	56.22	1.07	1095	1051	56.43	1.05	bCH(72), Rtrigd(20)
19	1009(vw)	1010(vw)	1029	988	2.01	2.54	1029	988	2.23	2.85	bCH(71), Rsymd(18)
20	984(w)	-	1000	960	1.02	0.26	1000	960	0.93	0.28	bCH(70), Rasymd (21)

21	927(ms)	927(w)	937	900	33.93	9.05	937	900	34.24	9.09	ωCH(66), ωCC(19)
22	903(ms)	898(vw)	926	889	13.12	0.52	925	888	13.15	0.43	ωCH(65),tNO_2(21)
23	844(vs)	842(s)	855	821	38.02	0.20	856	821	38.17	0.32	bCO(68), bCH(22)
24	812(ms)	-	841	807	24.95	26.24	841	807	24.96	26.27	ωCH(66), ωCC(19)
25	774(w)	775(w)	792	760	3.74	2.09	792	760	3.71	2.12	ωCH(64), NO_2wag(22)
26	756(s)	759(w)	771	740	6.34	1.47	771	740	6.24	1.46	NO_2sci(69), Rtrigd(18)
27	712(s)	715(w)	725	696	35.88	1.74	725	696	36.30	1.77	Rsymd(65), Rtrigd(16)
28	685(ms)	684(w)	688	660	5.15	2.12	687	660	4.70	2.08	Rtrigd(68), bCN(17)
29	626(vs)	626(w)	640	614	15.99	1.89	640	614	15.96	1.88	Rasymd(67), Rtrigd(16)
30	561(s)	561(vw)	569	546	11.08	1.08	569	546	10.94	1.10	NO_2rock(63), bCC(21)
31	526(s)	528(w)	533	511	10.04	1.27	533	511	9.87	1.18	bCN(61),bCF(23)
32	-	447(w)	453	435	0.43	0.20	452	434	0.42	0.20	tRsymd(58), ωCN(22)
33	-	395(w)	401	385	3.25	1.42	401	385	3.31	1.43	tRasymd(60), ωCC(17)
34	-	341(ms)	392	376	2.26	3.93	391	376	2.22	3.91	tRtrigd(59),bCF(22)
35	-	332(vw)	337	323	0.69	5.08	337	323	0.73	5.08	bCC(66), bCC(22)
36	-	244(vw)	332	318	4.76	1.50	332	319	4.59	1.53	bCF(58), bCO(18)
37	-	208(w)	238	228	2.84	0.50	238	228	2.85	0.50	ωCO(62), tRasymd(11)
38	-	190(vw)	206	198	2.71	0.73	206	198	2.63	0.77	NO_2wag (62), ωCH(28)
39	-	154(s)	159	153	9.45	0.43	159	153	9.43	0.43	ωCN(57), ωCO(21)
40	-	113(s)	126	121	0.80	3.60	125	120	0.80	3.63	ωCC(58), ωCO(19)
41	-	78(ms)	93	89	11.82	0.68	93	89	11.79	0.70	ωCF(59), ωCO(20)
42	-	-	46	44	0.46	1.66	46	44	0.45	1.65	tNO_2(56)

Table 3 Molecular orbital contributions of 4-fluoro-3- nitrobenzaldehyde

TDDFT/ B3LYP/6-311++G(d,p) Method				
Energy(eV)	**Oscillator strength**	**Wavelength (nm)**	**Major contributions**	**Assignment**
3.0266	0.0000	409.65	H-4 → L (78%)	π→π*
3.1008	0.0041	399.85	H-2 → L (92%)	π→π*
3.2639	0.0000	379.86	H→ L+1 (82%)	π→π*

Table 4 NBO analysis for 4-fluoro-3-nitrobenzaldehyde

Donor (i)	ED (i) (e)	Acceptor (j)	ED (j) (e)	Interaction Energy E(2) (kJ mol^{-1})	Energy difference E(j)–E(i) (a.u.)	Fock matrix element F (i,j) (a.u.)
π (C_1 - C_2)	0.81857	π^*(C_3 – C_4)	0.20470	9.16	0.26	0.062
		π^*(C_5 – C_6)	0.13377	10.70	0.29	0.072
		π^*(C_7 – O_8)	0.04878	9.39	0.29	0.070
π(C_3 – C_4)	0.82108	π^*(C_1 – C_2)	0.16794	11.43	0.31	0.076
		π^*(N_{11} – O_{12})	0.31401	10.18	0.17	0.056
π(C_5 – C_6)	0.82979	π^*(C_3 – C_4)	0.20470	13.42	0.26	0.076
n2(O_8)	0.93833	σ^*(C_1 – C_7)	0.03096	9.22	0.70	0.103
		σ^*(C_7 – H_9)	0.03254	11.44	0.62	0.108
n2(O_{12})	0.94713	σ^*(C_3 – N_{11})	0.05203	6.60	0.55	0.076
		σ^*(N_{11} – O_{13})	0.02954	9.18	0.73	0.104
n2(O_{13})	0.94778	σ^*(C_3 – N_{11})	0.05203	6.72	0.55	0.077
		σ^*(N_{11} – O_{12})	0.03165	9.61	0.72	0.106
		π^*(N_{11} – O_{12})	0.31401	85.42	0.15	0.142
n2(F_{14})	0.98389	σ^*(C_3 – C_4)	0.01827	3.81	0.95	0.076
		σ^*(C_4 – C_5)	0.01263	2.95	0.96	0.067
n3(F_{14})	0.95251	π^*(C_3 – C_4)	0.20470	11.41	0.42	0.095
π^*(C_3 - C_4)	0.20470	π^*(C_1 – C_2)	0.16794	59.68	0.03	0.081
		π^*(C_5 – C_6)	0.13377	52.04	0.03	0.082
σ^*(N_{11} – O_{12})	0.03165	σ^*(N_{11} – O_{13})	0.02954	10.80	0.01	0.055
π^*(N_{11} – O_{12})	0.31401	π^*(C_3 – C_4)	0.20470	8.39	0.12	0.055
		σ^*(N_{11} – O_{12})	0.03165	1.39	0.55	0.060

Table 5 The thermodynamic parameters of 4-fluoro-3-nitrobenzaldehyde

Parameters	Method/Basis set	
	B3LYP/ 6-31+G(d,p)	**B3LYP/6-311++G(d,p)**
Optimized global minimum Energy (Hartrees)	-649.48592104	-649.48607104
Heat capacity, C_v (cal mol^{-1} K^{-1})	35.582	35.587
Total energy(thermal), E_{total} (kcal mol^{-1})	70.979	70.973
Entropy, S (cal mol^{-1} K^{-1})		
Total	98.954	98.963
Translational	41.282	41.282
Rotational	30.788	30.788
Vibrational	26.884	26.892
Vibrational energy, E_{vib} (kcal mol^{-1})	69.202	69.196
Zero point vibrational energy, (kcal mol^{-1})	64.84506	64.83830
Dipole moment (Debye)	2.3623	2.3656
Rotational constants (GHz)		
A	1.76628	1.76610
B	0.63259	0.63263
C	0.47266	0.47262

Table 6 Mulliken's atomic charges of 4-fluoro-3-nitrobenzaldehyde

ATOM	Mulliken's atomic charges	
	B3LYP/ 6-31+G(d,p)	**B3LYP/ 6-311++G(d,p)**
C1	0.8300	1.1489
C2	-0.4435	-0.6664
C3	0.0539	-0.0969
C4	-0.2201	-0.4356
C5	0.0269	0.2591
C6	-0.1461	-0.4610
C7	-0.0570	-0.0408
O8	-0.2508	-0.2298
H9	0.1141	0.1486
H10	0.1700	0.2449
N11	-0.2518	-0.2027
O12	-0.0036	-0.0104
O13	0.0281	0.0314
F14	-0.1259	-0.1186
H15	0.1568	0.2285
H16	0.1728	0.2010

Table 7 ^{13}C and ^{1}H NMR chemical shifts for 4-fluoro-3-nitrobenzaldehyde

^{13}C Assignment	**Calculated Shift B3LYP/ 6-311++G(d,p) (ppm)**	**^{1}H Assignment**	**Calculated Shift B3LYP/ 6-311++G(d,p) (ppm)**
7C	191.73	9H	10.14
4C	168.54	10H	8.55
3C	145.99	16H	8.44
6C	138.29	15H	7.38
1C	137.54		
2C	137.48		
5C	123.30		

Table 8 ADMET profile of 4-fluoro-3-nitrobenzaldehyde

ADMET prediction	Value	ADMET prediction	Value
CaCo-2 permeability (log Papp in 10^{-6} cm/s)	1.296	P-glycoprotein substrate	No
Intestinal absorption (human) (%)	94.423	P-glycoprotein I inhibitor	No
Skin Permeability (log Kp)	-2.36	P-glycoprotein II inhibitor	No
VDss (human) (log L/kg)	-0.216	Total Clearance (log ml/min/kg)	0.502
Fraction unbound (human) (Fu)	0.294	Renal OCT2 substrate	No
BBB permeability (log BB)	-0.236	AMES toxicity test	Yes
CNS permeability (log PS)	-2.296	Max. tolerated dose (human) (log mg/kg/day)	0.866
CYP2D6 substrate	No	hERG I inhibitor	No
CYP3A4 substrate	No	hERG II inhibitor	No
CYP1A2 inhibitior	Yes	Oral Rat Acute Toxicity (LD50) (mol/kg)	2.294
CYP2C19 inhibitior	No	Oral Rat Chronic Toxicity (LOAEL) (log mg/kg_bw/day)	1.692
CYP2C9 inhibitior	No	Hepatotoxicity	No
CYP2D6 inhibitior	No	Skin Sensitisation	Yes
CYP3A4 inhibitior	No	T.Pyriformis toxicity (log ug/L)	0.617
Carcinogenicity	Non-	Minnow toxicity	1.351

	carcinogens	(log mM)	

Table 9(a) Binding energy (kcal/mol) of 4-fluoro-3-nitrobenzaldehyde with ALDHs inhibitor

Protein	Binding Energy	Ligand Efficiency	Inhibit Constant	Internal energy	vdw hb dissolve energy	Electrostatic Energy	Total Internal	Torsional Energy	Unbound Energy
ALDH1A3 (ID:5FHZ)	-6.0	-0.51	62.1	-6.31	-5.58	-0.34	-0.22	-1.11	-0.3
ALDH3A1 (ID:4H80)	-5.8	-0.41	56.1	-4.31	-4.68	-0.44	-0.12	-1.00	-0.2

Table 9(b) Docking calculation showing binding site residues, interacting residues and atoms in H-bonding

S.No.	Protein	Interacted Residues	Ligand and Protein in H-bonding
1	ALDH1A3 (ID:5FHZ)	PRO C:157, ARG B:167	THR C:155, GLY B:153, HIS B:168, ARG B:96
2	ALDH3A1 (ID:4H80)	SER G:422, LEU G:104, PRO G:205	GLY C:405, HIS G:423

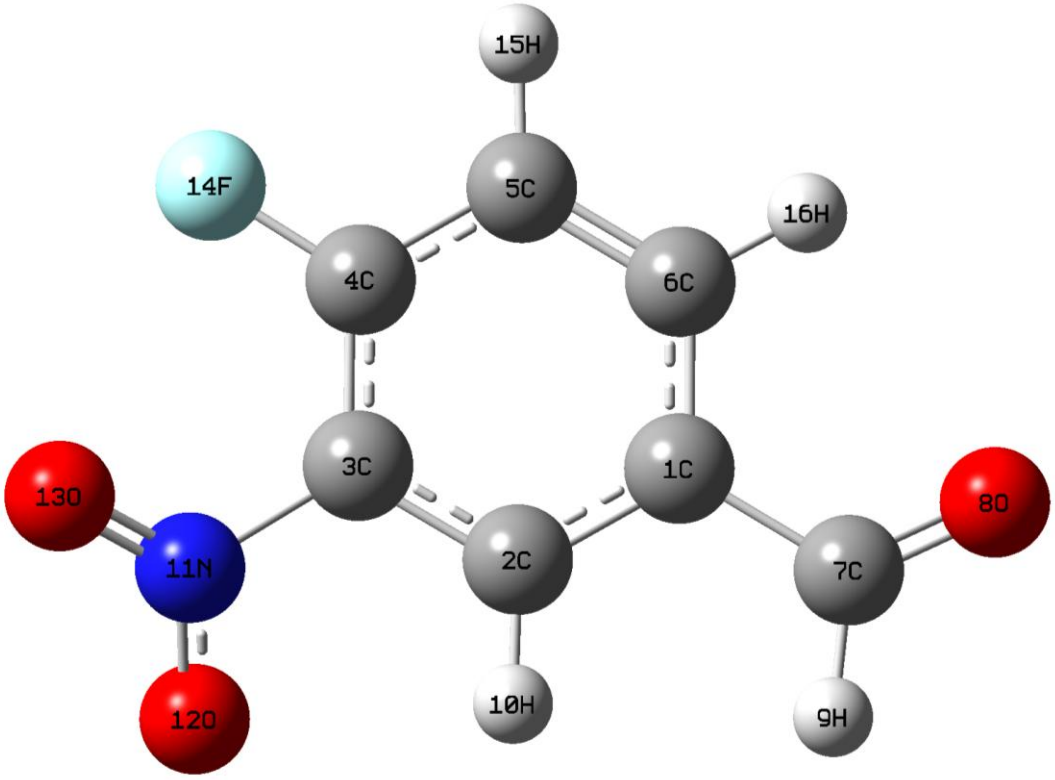

Fig. 1: Optimized structure of 4-fluoro-3-nitrobenzaldehyde

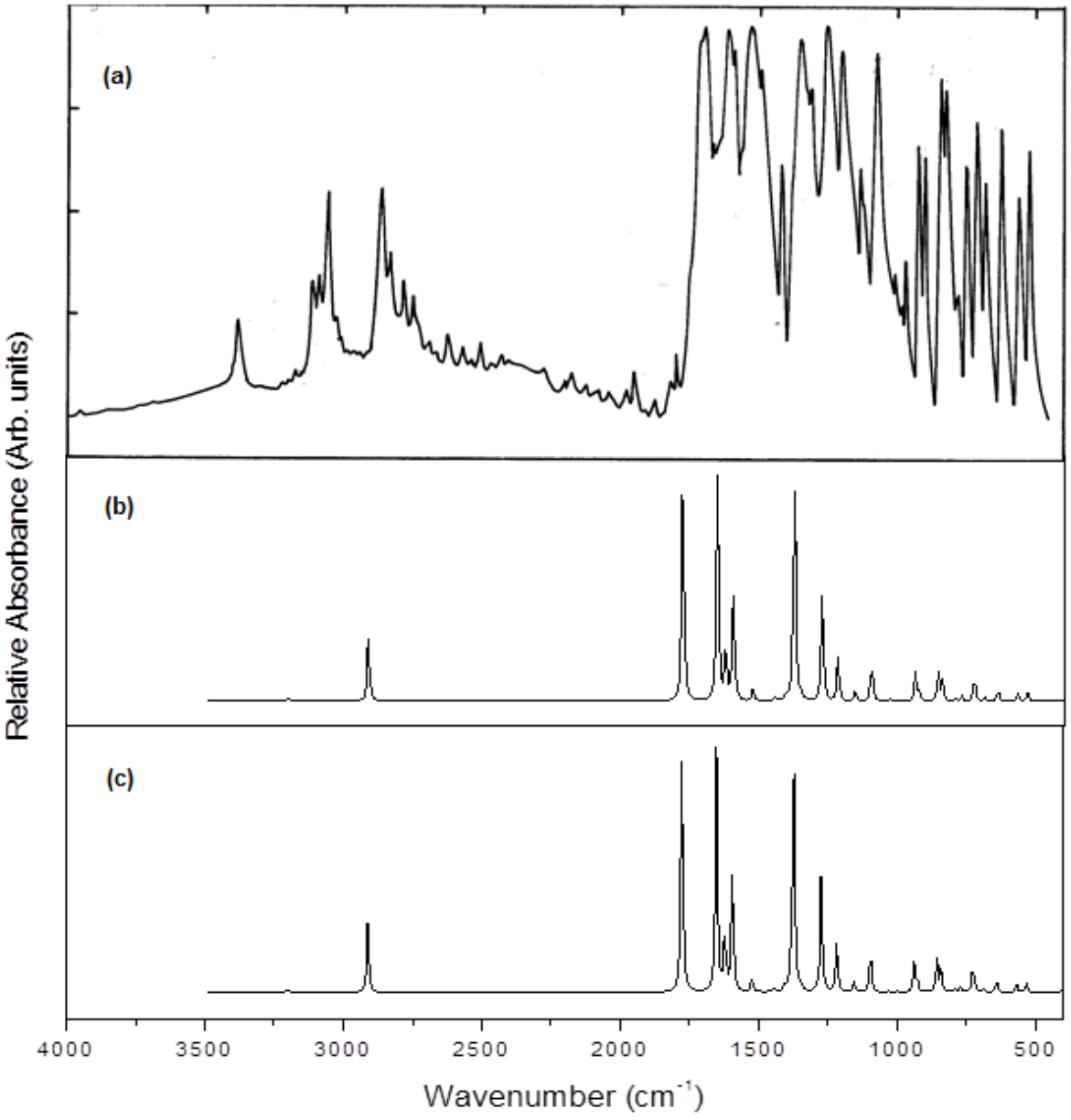
(a)
(b)
(c)
Relative Absorbance (Arb. units)
4000
3500
3000
2500
2000
1500
1000
500
Wavenumber (cm-1)

Fig. 2: Comparison of FTIR spectra of 4-fluoro-3-nitrobenzaldehyde (a) observed; (b) B3LYP/6-31+G(d,p); and (c) B3LYP/6-311++G(d,p).

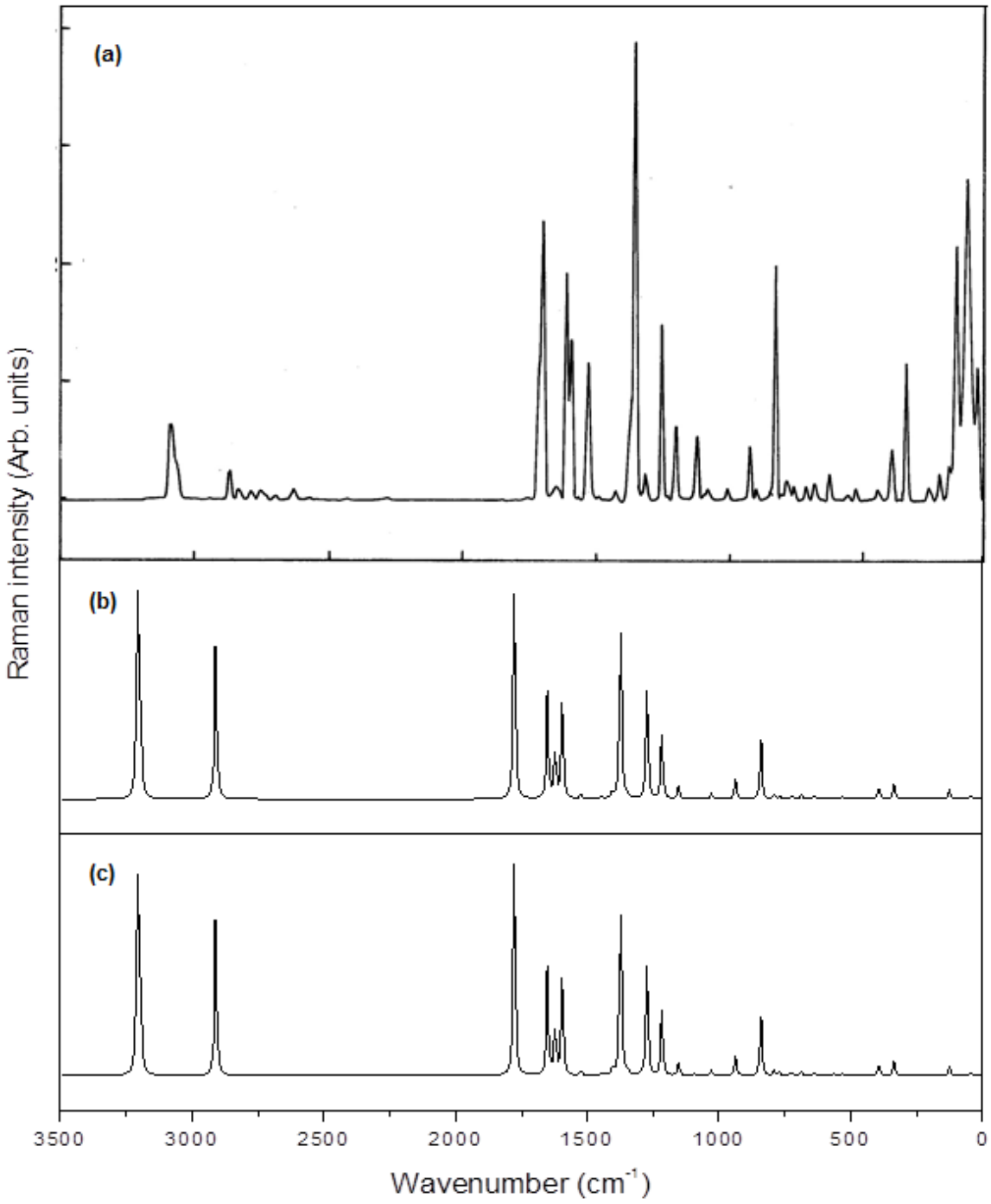

Fig.3: Comparison of FT-Raman spectra of 4-fluoro-3-nitrobenzaldehyde (a) observed; (b) B3LYP/6-31+G(d,p); and (c) B3LYP/6-311++G(d,p).

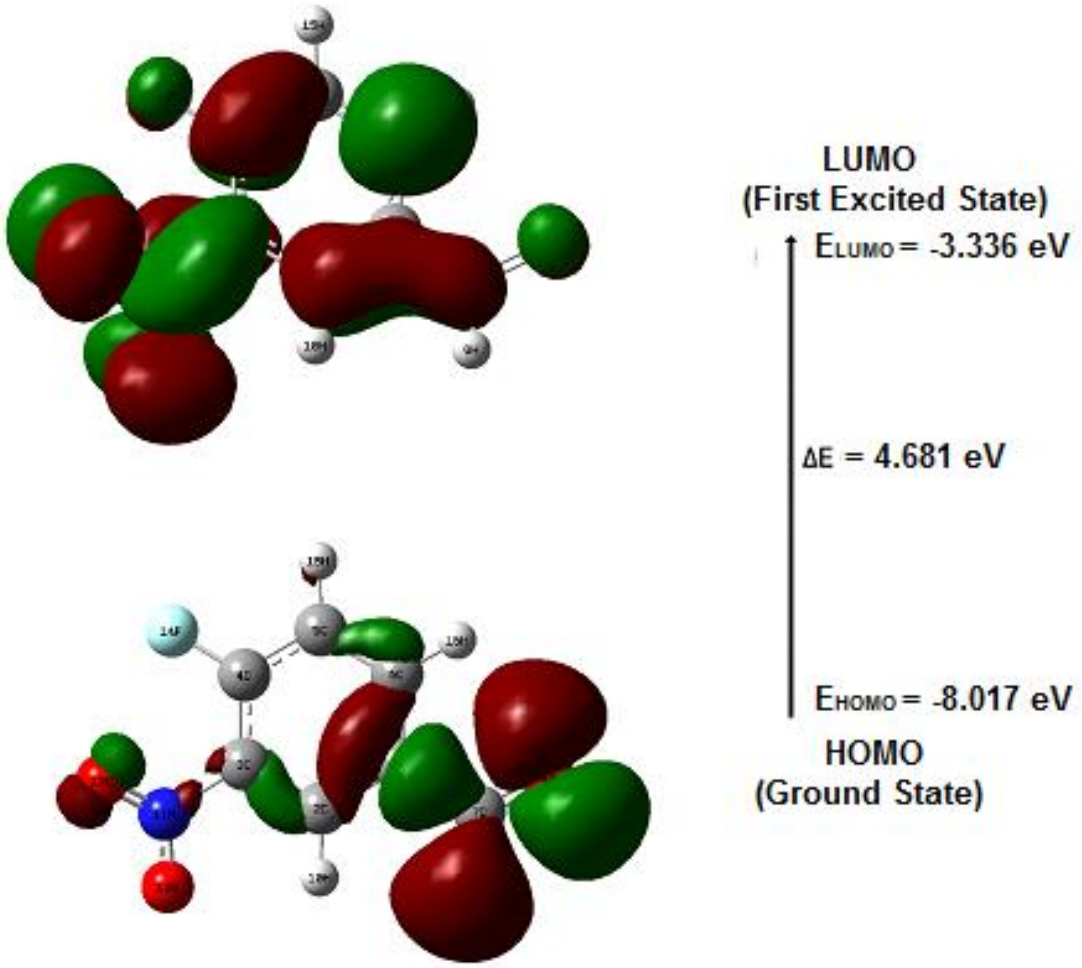

Fig. 4: Frontier molecular orbitals of 4-fluoro-3-nitrobenzaldehyde

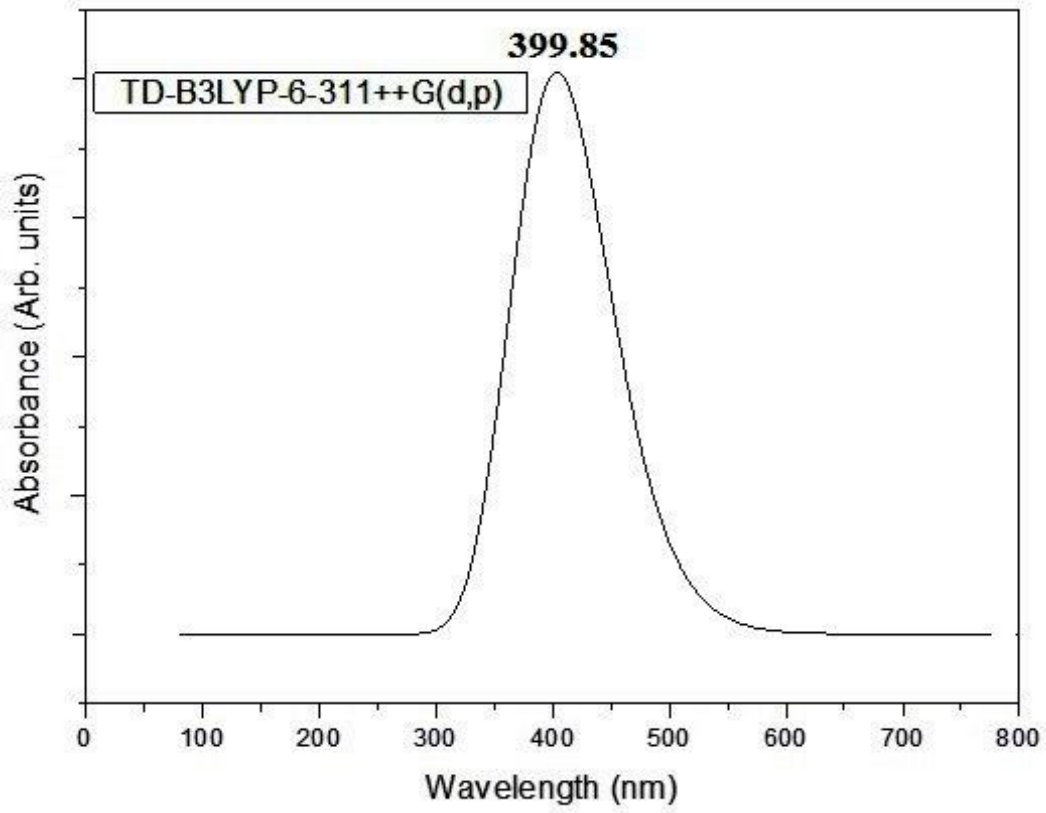

Fig. 5: UV plot for 4-fluoro-3-nitrobenzaldehyde

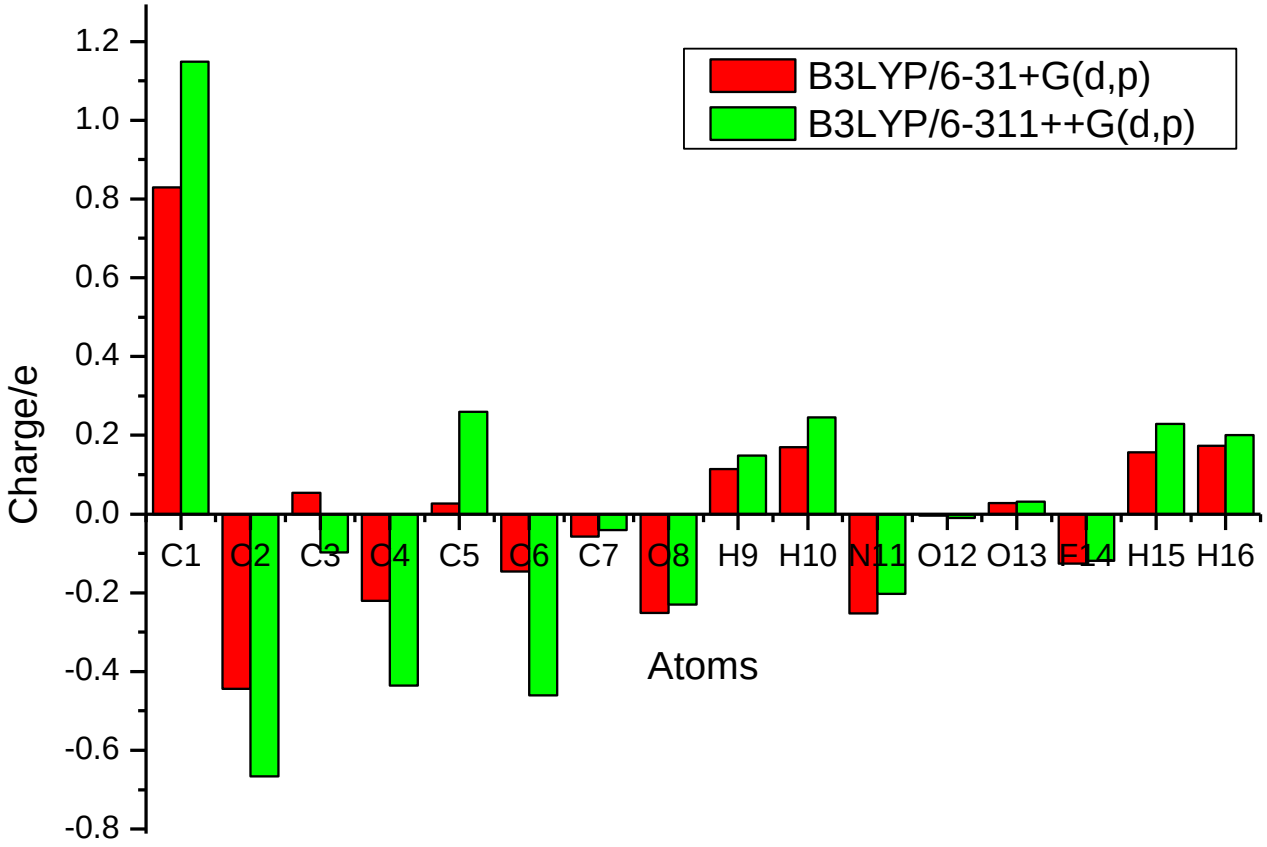

Fig. 6: Mullikan charges for 4-fluoro-3-nitrobenzaldehyde

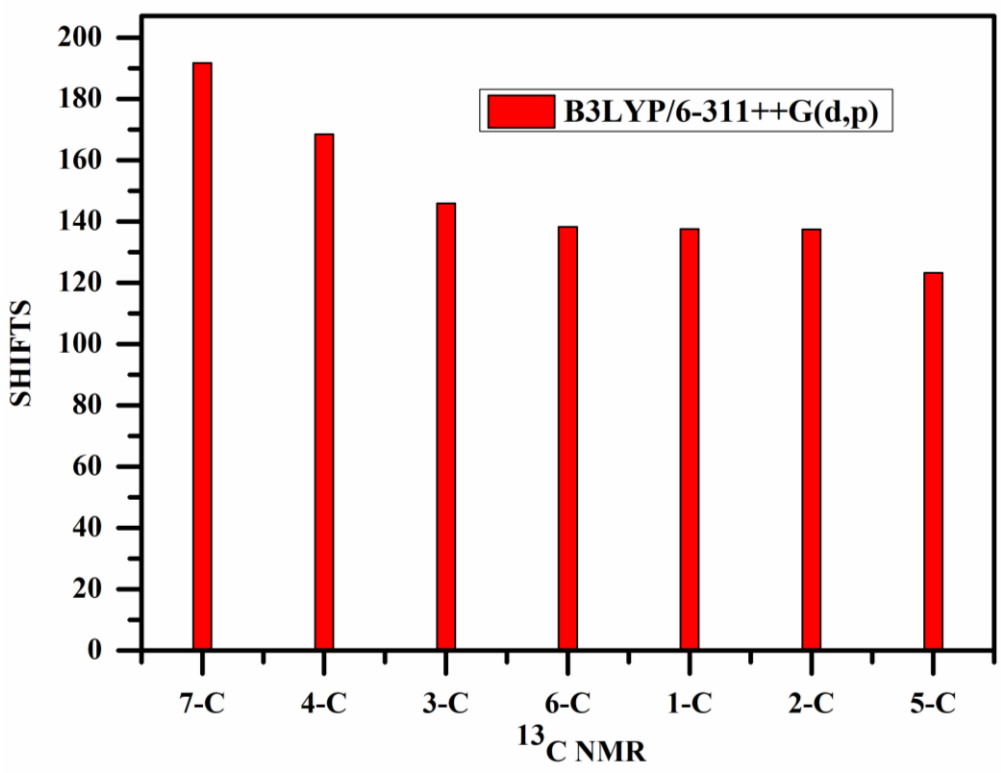
B3LYP/6-311++G(d,p)
SHIFTS
200
180
160
140
120
100
80
60
40
20
0
7-C
4-C
3-C
6-C
1-C
2-C
5-C
13C NMR

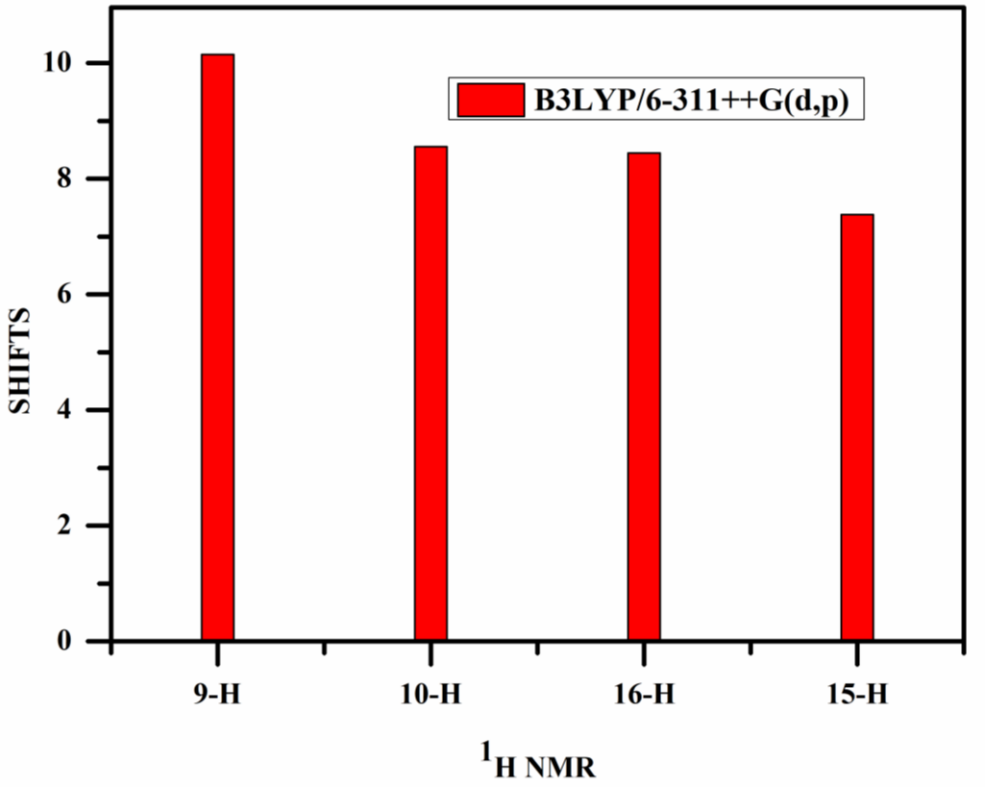
B3LYP/6-311++G(d,p)
SHIFTS
10
8
6
4
2
0
9-H
10-H
16-H
15-H
1H NMR

Fig. 7: ^{13}C and ^{1}H NMR plot for 4-fluoro-3-nitrobenzaldehyde

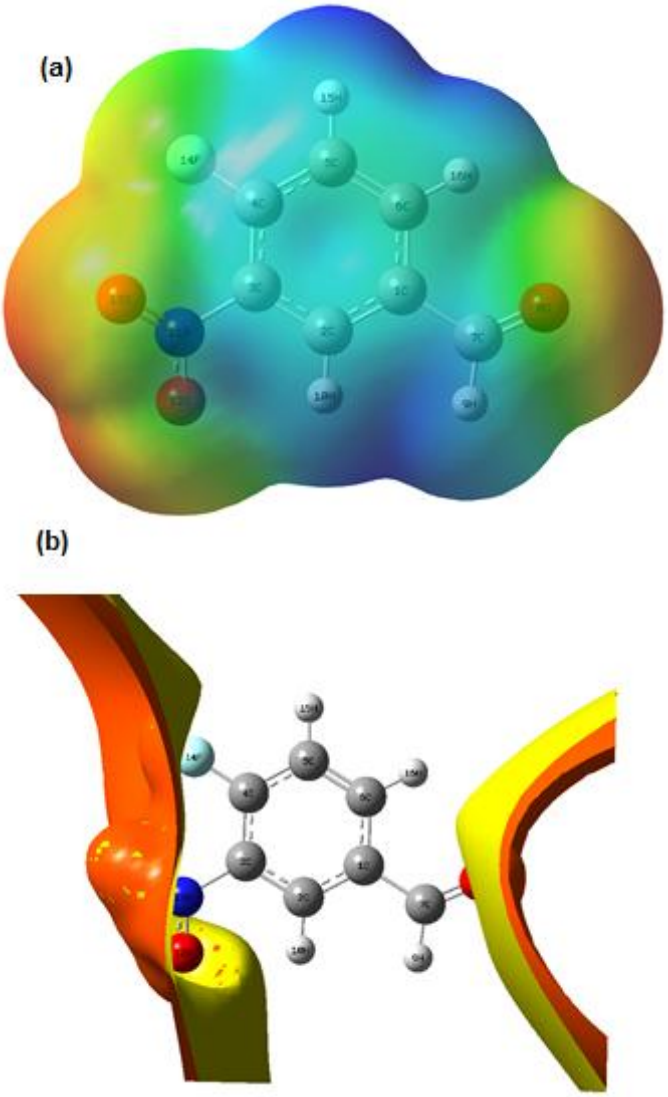

Fig. 8: (a) MEP; (b) ESP map for 4-fluoro-3-nitrobenzaldehyde

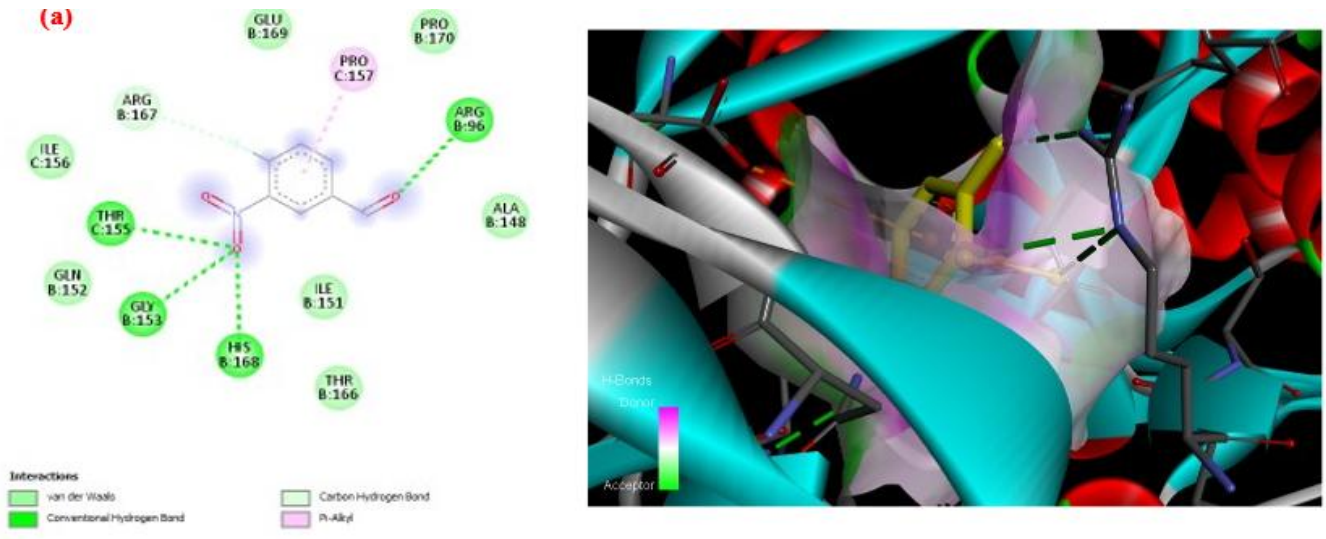

Fig. 9: (a) 2D and 3D structure of Protein ALDH1A3 interactions with ligand 4-fluoro-3-nitrobenzaldehyde

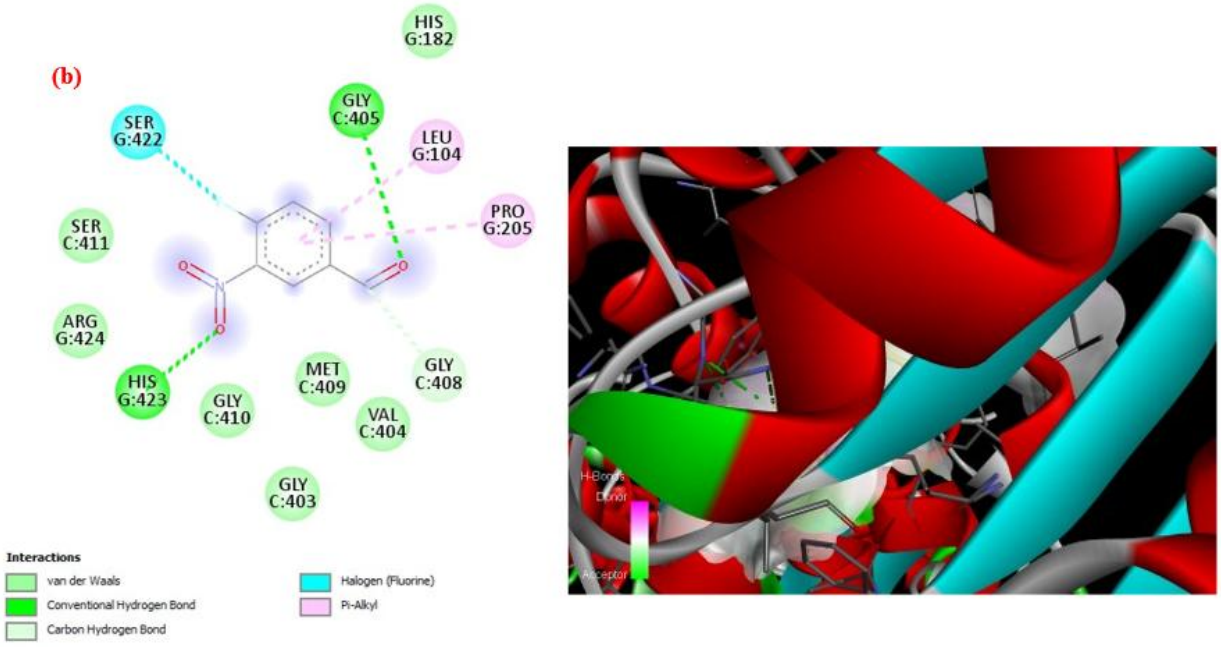

Fig. 9: (b) 2D and 3D structure of Protein ALDH3A1 interactions with ligand 4-fluoro-3-nitrobenzaldehyde